JOURNAL OF MAGNETIC RESONANCE **124,** 383–392 (1997)
ARTICLE NO. MN961016

HECADE: HMQC- and HSQC-Based 2D NMR Experiments for Accurate and Sensitive Determination of Heteronuclear Coupling Constants from E.COSY-Type Cross Peaks

WIKTOR KOŹMIŃSKI* AND DANIEL NANZ†

Organisch-chemisches Institut, Universität Zürich, Winterthurerstrasse 190, CH-8057 Zürich, Switzerland

Received August 16, 1996; revised September 23, 1996

Two-dimensional pulse sequences for the determination of heteronuclear long-range coupling constants are presented. The sequences are based on the HMQC/HMBC or HSQC technique with subsequent optional homonuclear I-spin transfer. However, they yield tilted cross-peak patterns displaying antiphase heteronuclear coupling constants in the projections of both dimensions, which allow accurate determination of the couplings even in cases where the linewidth is of comparable magnitude. Two characteristic pulse-sequence elements were implemented to shape the F_1 domain: the first element allows an arbitrary scaling of the heteronuclear coupling splittings relative to S-spin chemical-shift differences, whereas the second element achieves homonuclear broadband decoupling among the I spins in the HMQC/HMBC experiments and thus allows purely absorptive representations of such spectra. In comparison with established (ω_1) X-half-filtered TOCSY spectra, the signal dispersion in F_1 is significantly improved and largely under experimental control. Furthermore, heteronuclear couplings of (I_1, S) pairs where S is either quaternary or carries one or more I spins that do not belong to the same I-coupling network as I_1 can also be measured. The implementation of pulsed field gradients results in good suppression of spectral artifacts.

INTRODUCTION

Heteronuclear coupling constants, especially vicinal three-bond couplings, provide valuable restraints for the characterization of molecular conformation, bonding, and dynamics (*1*). Ideally, methods that are used to determine small coupling constants from splittings in 2D spectra generate E.COSY-type multiplet patterns (*2*). In this article, we present new sequences of this type that are based on the HMQC (*3–5*)/HMBC (*6*) or the HSQC (*7*) experiment. Methods have been developed to tilt the cross-peak pattern displaying the active coupling. Thus, the advantage of E.COSY-type peak patterns is also available in two-spin systems. No additional passive spin is required. Purely absorptive phase in both dimensions and broadband homonuclear I-spin decoupling in the F_1 domain are achieved. The F_1 domain encodes *a*rbitrarily *s*caled *s*hift and *c*oupling *i*nformation (ASSCI), namely S-spin chemical-shift differences and heteronuclear coupling splittings that can be scaled to optimize signal dispersion and resolution. Sequences that allow a long-range (I → S) transfer are also presented. The new pulse sequence family is called HECADE (*he*teronuclear *c*ouplings from *a*SSCI-*d*omain Experiments with *e*.COSY-type cross peaks).

The starting point for this work was the intention to improve the (ω_1) X-half-filtered TOCSY family of pulse sequences (HETLOC) for the determination of heteronuclear coupling constants (*8, 9*). The corresponding spectra display E.COSY-type cross-peak patterns but also have the following disadvantages: (i) Signal overlap due to homonuclear coupling evolution in two dimensions which also produces mixed phases that can be purged only with concomitant reduction in signal intensity. For nongeminal couplings this problem might be solved by placing a $BIRD_y$ pulse in the center of t_1 (*10, 11*). (ii) Signal overlap caused by the inherent small chemical-shift range of the I-spin when I is a proton. (iii) Artifact suppression, i.e., the rejection of signals from undesired isotopomers, is difficult to achieve. Established approaches include a BIRD relaxation filter (*12*) that requires uniform relaxation times for good results (*8, 9, 13*) as well as gradient-assisted X half-filters (*14*), which yield clean spectra at the expense of a signal loss by a factor of two (*15*). (iv) Difficult spectrum interpretation and possibly unfortunate signal overlap due to relatively large ^1J(I, S) splittings. (v) Missing cross peaks between (I_1, S) pairs where S is either quaternary or carries one or more I spins that do not belong to the same I spin coupling network as I_1.

The sequences proposed in the following achieve improvements for most of these points by combining partly new pulse-sequence elements with a careful reconstruction of tilted cross-peak patterns. Two pulse-sequence elements that we call ASSCI and HECSII are discussed. The HECSII element is then shown to allow the measurement of HMQC/

* Present address: Department of Chemistry, Warsaw University, ul. Pasteura 1, 02-093 Warszawa, Poland.

† Present address: Universitätsspital Zürich, Departement für Medizinische Radiologie, Magnetresonanz-Zentrum, Rämistrasse 100, CH-8091 Zürich, Switzerland.

1090-7807/97 $25.00

HMBC spectra with pure phases. The HMQC- and subsequently the HSQC-based pulse sequences for the measurement of heteronuclear couplings are discussed and compared. A summary of the evaluation of the sequences and guidelines for the choice of the appropriate sequence are given in the Conclusions.

FREQUENCY DOMAIN ENCODING ARBITRARILY SCALED SHIFT AND COUPLING INFORMATION (ASSCI DOMAIN)

In the present work, pulse sequences are designed to evolve a shift and a heteronuclear coupling sequentially in separated and synchronously incremented time periods. The corresponding modulations are transformed by means of a Fourier transformation and represented in a single frequency domain. The increments of the shift and coupling evolution time can be chosen arbitrarily within the limits set by relaxation. This allows arbitrary scaling of the interactions in the spectrum, thus avoiding problems with digital resolution and/or signal overlap. In addition, couplings can be combined with the shift evolution of a nucleus that is not one of the coupling partners. This provides maximum flexibility in choosing a well-resolved frequency domain, in contrast to a scaling performed in a single evolution period by means of a π pulse (*13*).

The technique of monitoring *n* different evolutions of a spin system indirectly in *n* sequential time periods (t_i and t_i* in Fig. 1a) that are incremented synchronously and combining the information into *n*-1 frequency domains has been called Accordion spectroscopy (*16, 17*). Apart from encoding a single-quantum evolution together with the progress of a chemical-exchange (*16, 17*) or relaxation process (*18, 19*) the chemical-shift evolution of two different nuclei (*20–23*) was also monitored in this way. When combining a chemical shift with a coupling into a common frequency domain the appearance of the spectrum does not depend on the absolute sign of the coupling constant. It is therefore sufficient to observe a sine or cosine component of the coupling evolution and thus obtain purely absorptive 2D spectra with standard techniques. We have previously shown that the ASSCI-domain approach can successfully be applied to measure homonuclear S-spin couplings indirectly via I spins (*24, 25*). Recently, it was also employed for the measurement of long-range CH coupling constants (*26*).

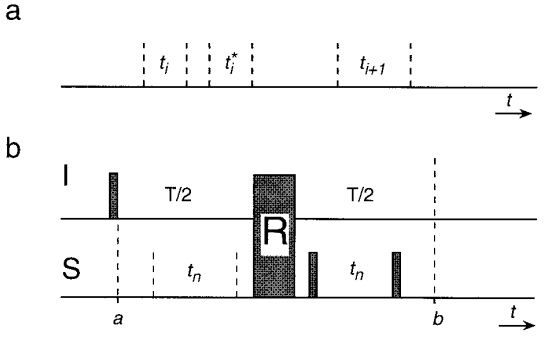

FIG. 1. Basic and general scheme of two pulse-sequence elements employed. (a) Accordion spectroscopy. In the present case the frequency domain ω_i encodes arbitrarily scaled shift and coupling information (ASSCI domain). The corresponding chemical shift and coupling evolve during t_i and t_i*, or vice versa. (b) HMQC evolution compensated for spin interactions of I nuclei (HECSII): I-spin homonuclear coupling and optionally I-spin chemical-shift evolution between points *a* and *b* are refocused by the element *R*, as described in the text.

HMQC EVOLUTION COMPENSATED FOR SPIN INTERACTIONS OF I NUCLEI FOR PURE-PHASE SPECTRA (HECSII)

The main disadvantage of the HMQC experiment is that the heteronuclear double- and zero-quantum coherences evolve under the homonuclear I-spin couplings, which leads to phase distortions and a dispersion of signal intensity. For selective HMBC experiments it was recently shown how the intensity dispersion due to homonuclear I couplings, but not the phase distortion, can be avoided, however, at the expense of intensity dispersion due to heteronuclear couplings (*27*). Here, we suggest I-spin interaction-compensated HMQC evolution periods as a more general solution, as shown in Fig. 1b. The key feature consists of a refocusing element *R* that separates the overall I-spin evolution into two symmetrical halves and refocuses the homonuclear coupling evolution between points *a* and *b*. Other interactions, e.g., I-spin chemical shift and heteronuclear couplings, may or may not be refocused, depending on the experiment. Examples for useful elements *R* are the following: (i) A multiplet-selective I-spin π pulse which selectively inverts the spin states of a single I spin. Among the advantages of this implementation is the possibility of realizing efficient heteronuclear long-range transfers, as described below. (ii) A spectral-region-selective I-spin π pulse acting on protons which do not exhibit mutual couplings, e.g., the NH protons of a peptide, in which S = ^{15}N or ^{13}C, whether at natural abundance or enriched. Here, also efficient long-range transfers are feasible. (iii) BIRD pulses (*10, 28, 29*). BIRD$_x$ pulses refocus I-spin chemical shift and homonuclear but not heteronuclear couplings whereas BIRD$_y$ pulses refocus the I-spin homonuclear and heteronuclear couplings. This implementation does not refocus geminal homonuclear couplings, e.g., of diastereotopic methylene protons. Note, however, that the resulting phase distortion in the applications presented below is not detrimental since both peaks relevant for the coupling-constant evaluation experience the same phase distortion. For peptides, the BIRD element may be especially useful with S = ^{15}N, whether enriched or at natural abundance. Not only efficient transfers to nitrogen but also long-range transfers to carbon nuclei could be feasible in triple-resonance experiments of enriched compounds. Depending on the application, the refocusing element *R* will cause a coherence-order change Δp of either ± 2 or 0. The suppression of undesired

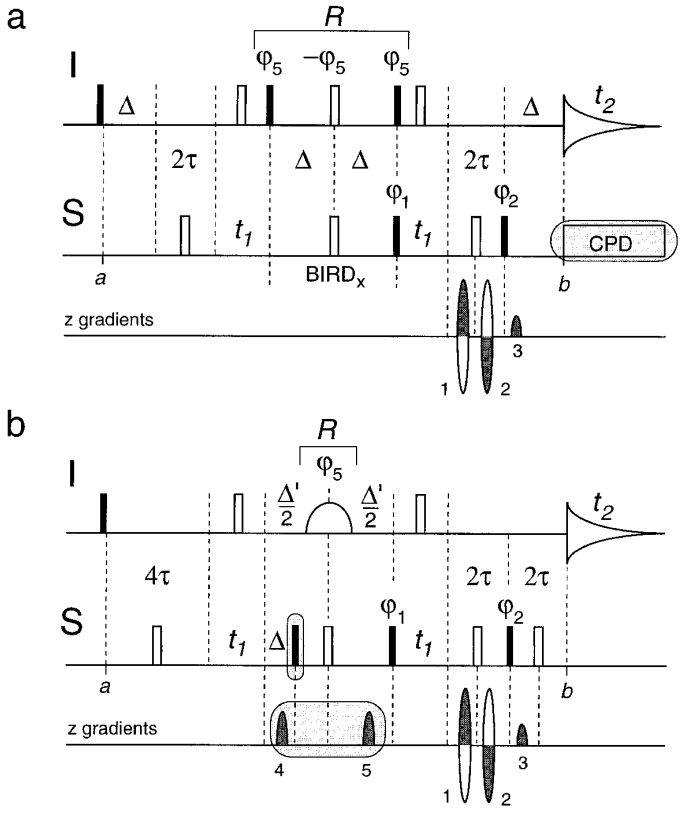

FIG. 2. HECSII–HMQC (a) and HECSII–HMBC (b) pulse sequences yielding purely absorptive 2D spectra with broadband homonuclear I-spin decoupling in the F_1 domain. Sequence (a) represents a heteronuclear one-bond correlation experiment, whereas with (b) long-range correlations of I spins inverted by the central refocusing I-spin pulse are observed. Dark-filled and white bars represent $\pi/2$ and π pulses, respectively. All pulses are applied along the x axis unless indicated differently. Δ and Δ' are set to $1/[2^1J(\mathrm{I,S})]$ and $1/[2^nJ(\mathrm{I,S})]$, respectively. The duration of a pulsed field gradient and of the subsequent recovery time amounts to τ. Echo and antiecho data sets were recorded with opposite sign of gradients 1 and 2 and processed accordingly (*44*, *45*). Pulse-sequence elements in lightly shaded boxes are optional. In (b) short-range cross peaks might be suppressed by the optional $\pi/2$(S) pulse [low-pass filter (6)]. In contrast to (a), where the heteronuclear coupling is refocused at point *b*, antiphase multiplets are obtained with (b). Phases were cycled as follows: φ_1: x, $-x$; φ_2: $2x$, $2(-x)$; receiver phase: x, $-x$, $-x$, x. The amplitude ratio of gradients 1, 2, and 3 is given by γ_I: $-\gamma_I$: $2\gamma_S$ for echo selection when γ_I and γ_S have the same sign. The two optional central gradient pulses in sequence (b) were applied with equal amplitude. A nongradient version of (a) could be obtained by omitting the two periods labeled 2τ, the corresponding π(S) pulses, and the gradient pulses.

signals might therefore be improved by appropriately cycling its phase, which is called φ_5 in the sequences shown below, and/or by flanking it with appropriate gradient pulses (*29*).

As a first example of HECSII implementations (*H*MQC *e*volution *c*ompensated for spin *i*nteractions of *I* nuclei for pure-phase spectra), consider the pure-phase HMQC and HMBC experiments shown in Fig. 2. In Fig. 2a heteronuclear one-bond couplings evolve during the first Δ. The first $\pi/2$(S) pulse excites heteronuclear multiple-quantum coherences which evolve during the subsequent t_1 period under the S-spin chemical-shift interaction. Heteronuclear coupling evolution during the delay Δ just prior to acquisition produces in-phase multiplets and allows decoupling the S spins during t_2. The BIRD_x pulse, placed in the center between I-spin excitation and the beginning of data acquisition, refocuses I-spin homonuclear couplings and chemical shifts in the isotopomers of interest. In order to keep the BIRD element at this central point in time during the course of the experiment, t_1 must be compensated prior to the HMQC evolution. However, because of the π(I) pulse, this first t_1 is a ''dummy'' evolution period, which does not lead to a modulation of the observed signal. The signal selection is supported by means of pulsed field gradients. Again, the gradient time 2τ must be compensated prior to the BIRD pulse in the first half of the experiment with a π(S) pulse to prevent heteronuclear coupling evolution. The pulse sequence 2b is aimed at achieving a heteronuclear long-range transfer of protons inverted by the selective or semiselective π pulse that divides the proton evolution into two halves. Δ' should be optimized for heteronuclear long-range coupling constants. Since the magnitude of such couplings varies, a nonrefocusing variant that yields the active couplings in antiphase in F_2 is presented.

For HSQC-based sequences, the homonuclear I-spin couplings cause problems only when an I-spin coherence is to evolve under a heteronuclear coupling. Here, the same refocusing elements *R* described above can be used.

HMQC-BASED HECADE PULSE SEQUENCES

The new HMQC-based sequences for the determination of heteronuclear coupling constants are displayed in Fig. 3. All sequences correlate an ASSCI domain which combines the S chemical shift with either a one-bond (a and c) or a long-range (b) heteronuclear coupling constant, with the I spectrum. Optional TOCSY transfer (*30*, *31*) increases the number of couplings that are observed, which, for sequences (a) and (c), is necessary for determining long-range coupling constants.

Common to all sequences is the central refocusing element between points *a* and *b* which ensures that the signals are not modulated by I-spin homonuclear coupling and chemical-shift evolution between these two points. In contrast to the original half-filtered TOCSY spectra, the states of the S spins are mixed prior to and following the S-spin chemical-shift evolution. This means that, without special precautions, the cross peaks will not show the favorable tilt of E. COSY or homonuclear *J*-resolved spectra but will display a symmetry in F_1. However, it is possible to reconstruct cross-peak patterns which allow heteronuclear coupling constants to be read from the spectrum even when the respective splitting is on the order of the linewidth.

In sequences (a) and (b) the relevant components of the density matrix at point *b* are adequately described by the following four Cartesian product-operator terms—assuming that $\Delta = 1/(2J_{\mathrm{IS}})$:

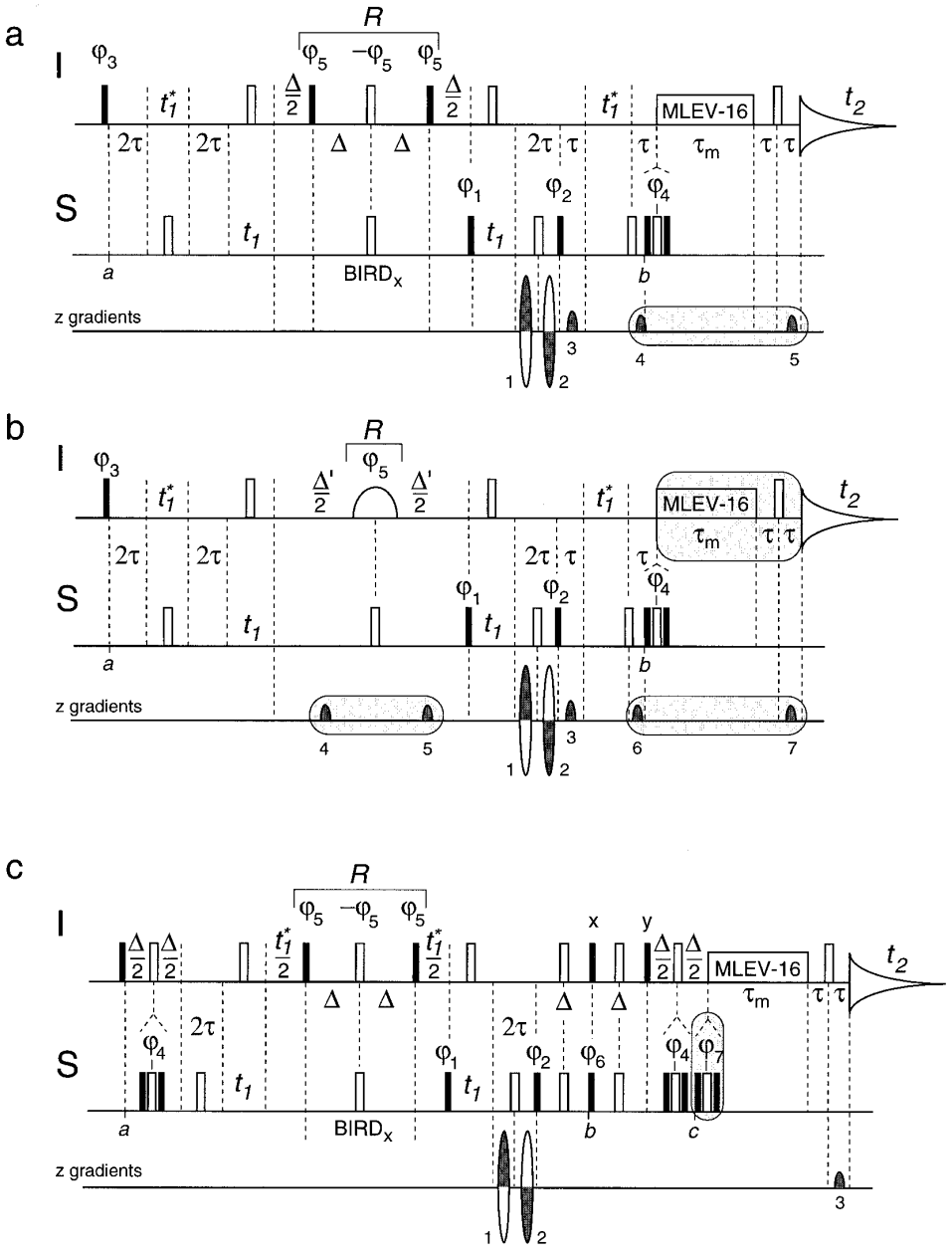

FIG. 3. HMQC-based (a, c) and HMBC-based (b) pulse sequences for the determination of heteronuclear coupling constants from tilted E.COSY-type cross peaks, phase sensitive using the echo–antiecho method. For an explanation of the pulse-sequence symbols, see the legend to Fig. 2. Phase cycles are listed in Tables 1 and 2. As in Fig. 2, sequence (a) achieves a heteronuclear single-bond transfer and sequence (b) achieves a multiple-bond transfer. Sequence (c) represents a variant of (a) with sensitivity enhancement. All sequences generate an ASSCI F_1 domain (cf. legend to Fig. 1 and text) that displays the active heteronuclear coupling splitting centered at the S-spin chemical-shift position. The relative magnitude of coupling and S-spin chemical-shift differences in F_1 can be scaled arbitrarily by varying the increment ratio of t_1^* and t_1. The central refocusing element R between points *a* and *b* achieves broadband homonuclear decoupling in F_1. The multiple-pulse sequence scheme of the optional isotropic mixing preserves the I-spin coherence orders. Thus, the mixing sequence can be flanked by gradient pulses without severe sensitivity loss (*46*).

$$
\begin{aligned}
A_1 &= \tfrac{1}{2} I_y \cos(\omega_S t_1)\sin(\pi J_{IS} t_1^*),\\
B_1 &= I_x S_z \cos(\omega_S t_1)\cos(\pi J_{IS} t_1^*)\\
A_2 &= \mp\tfrac{1}{2} I_x \sin(\omega_S t_1)\sin(\pi J_{IS} t_1^*),\\
B_2 &= \pm I_y S_z \sin(\omega_S t_1)\cos(\pi J_{IS} t_1^*).
\end{aligned}
\qquad [1]
$$

The sign of the terms A_2 and B_2 depends on the selection of the echo or antiecho signal by the pulsed field gradients, i.e., on the sign of gradient pulses 1 and 2. For each echo and antiecho data set at least four FIDs are coherently added with the pulse and receiver phases displayed in Table 1. Depending on phase $\varphi_4(-x$ or $-y)$ the last three S pulses

TABLE 1
Basic Phase Cycle for Experiments (a) and (b) in Figs. 3 and 6

Scan No.	φ_1	φ_3	φ_4	φ_R
1	0	0	2	0
2	0	0	3	0
3	1	1	2	2
4	1	1	3	0

Note. Each scan tabulated is recorded twice, once with echo and once with antiecho selection by the pulsed field gradients, respectively. The echo and antiecho data sets are stored in separate memory locations. ($\varphi_2 = \varphi_5 = 0$.)

act as either a composite 0 or a π pulse which is less prone to off-resonance effects (*32, 33*) than a $\pi/2(S)_x$, $\pm\pi/2(S)_x$ (*34*) element. Shifting φ_4 by $\pi/2$ inverts the sign of the antiphase *B* terms which are thus canceled in the first two scans (*35*). The *A*-term signals represent an antiphase/in-phase cross peak in F_1 and F_2, respectively, with pure phase, as depicted in Scheme 1a:

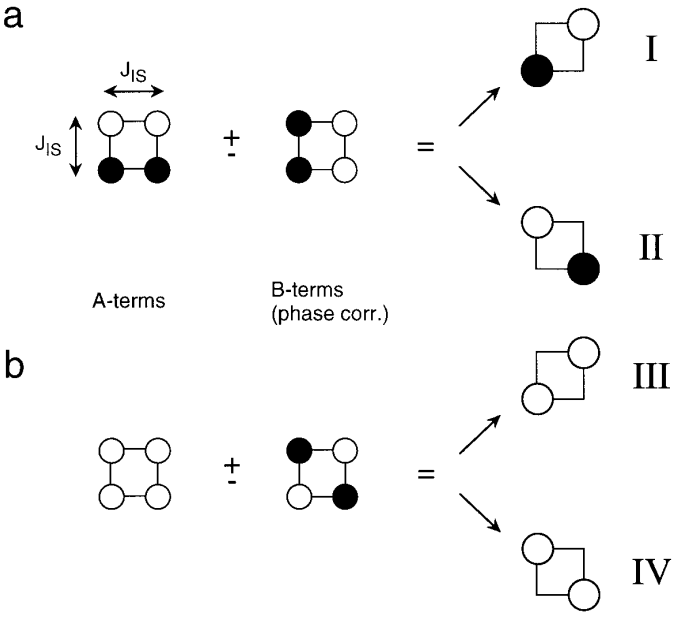

SCHEME 1

In the next two scans, the receiver phase is inverted in step with the cycling of φ_4 which leaves the *B* terms as observables. The phase of the *A* and *B* terms differs by $\pi/2$ in both dimensions which is accounted for by shifting φ_1 and φ_3. This basically exchanges the indices 1 and 2 of the terms in Eq. [1]. The signal obtained in these second two scans represents an in-phase/antiphase cross peak in F_1 and F_2, respectively. Upon addition of all four scans, the desired E.COSY-type multiplet is obtained. The phase cycles used were consistently adjusted to produce type I cross peaks (Scheme 1). Type II peaks could be obtained with a modified receiver-phase cycle to reverse the sign for the *B* terms. We decided not to refocus the heteronuclear coupling prior to acquisition in sequences 3a and 3b and 6a and 6b, described below, to avoid artifacts produced by nonuniform coupling constants and additional delays in sequences (b). In sequences 3c and 6c, all four cross-peak types of Scheme 1 can be obtained without modifications of the pulse sequences: to observe peak patterns (a), the net pulse angles of the first and second composite S pulse must be equal in 3c and must differ by π in 6c. Vice versa, to obtain peak patterns (b) these pulse angles must differ in 3c by π and must be equal in 6c.

Spectra measured with sequences 3a and 3b are shown in Figs. 4 and 5, respectively. Figure 4a displays a contour plot obtained with sequence 3a from a sucrose solution in D_2O. The sucrose structure and the numbering of the atoms is:

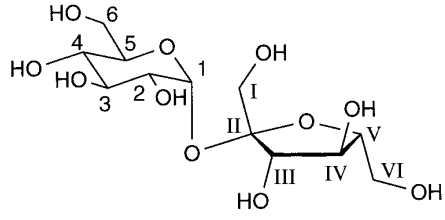

In order to illustrate the tilt of the cross-peak patterns, Fig. 4b shows an expansion of cross peaks of the anomeric proton. Note that homonuclear broadband I-spin decoupling is achieved in the F_1 domain. Further, in comparison with chemical-shift differences in the spectrum, the doublet splittings due to $^1J(^{13}C,^1H)$ couplings appear reduced by a factor of 2.5 to reduce signal overlap. The relative signs of the heteronuclear long-range and one-bond couplings are immediately evident from the tilt of the corresponding cross peaks. The heteronuclear coupling constants are preferably extracted from rows taken parallel to the F_2 dimension through the two doublet components.

The sequence in Fig. 3b represents a complementary experiment. Without the optional TOCSY transfer the heteronuclear coupling constants of the I spin inverted by the selective π pulse can be obtained—as long as $\sin(\pi J_{IS}\Delta')$ is sufficiently large. As an example Fig. 5 displays cross peaks of the anomeric proton in the sucrose sample. Note the coupling between H(1) and the quaternary carbon C(II) and also the well-resolved cross peaks with carbons C(3) and C(5) whose chemical shifts differ by only 0.18 ppm. Upon addition of the TOCSY transfer, the number of observed couplings in the selected isotopomers is significantly increased; in the present case at least 18 cross peaks were clearly observed in the corresponding spectrum compared to 6 without the TOCSY mixing.

The sequences discussed so far do not yield maximum theoretical signal intensity. However, sensitivity enhance-

ment (*36–39*) optimized for IS spin systems is implemented in sequence 3c. A basic phase-cycling scheme is shown in Table 2. For the first and second group of four scans in this cycle, the relevant product-operator terms excited at point *c* in the sequence are given by terms *A* and *B* of Eq. [2], respectively:

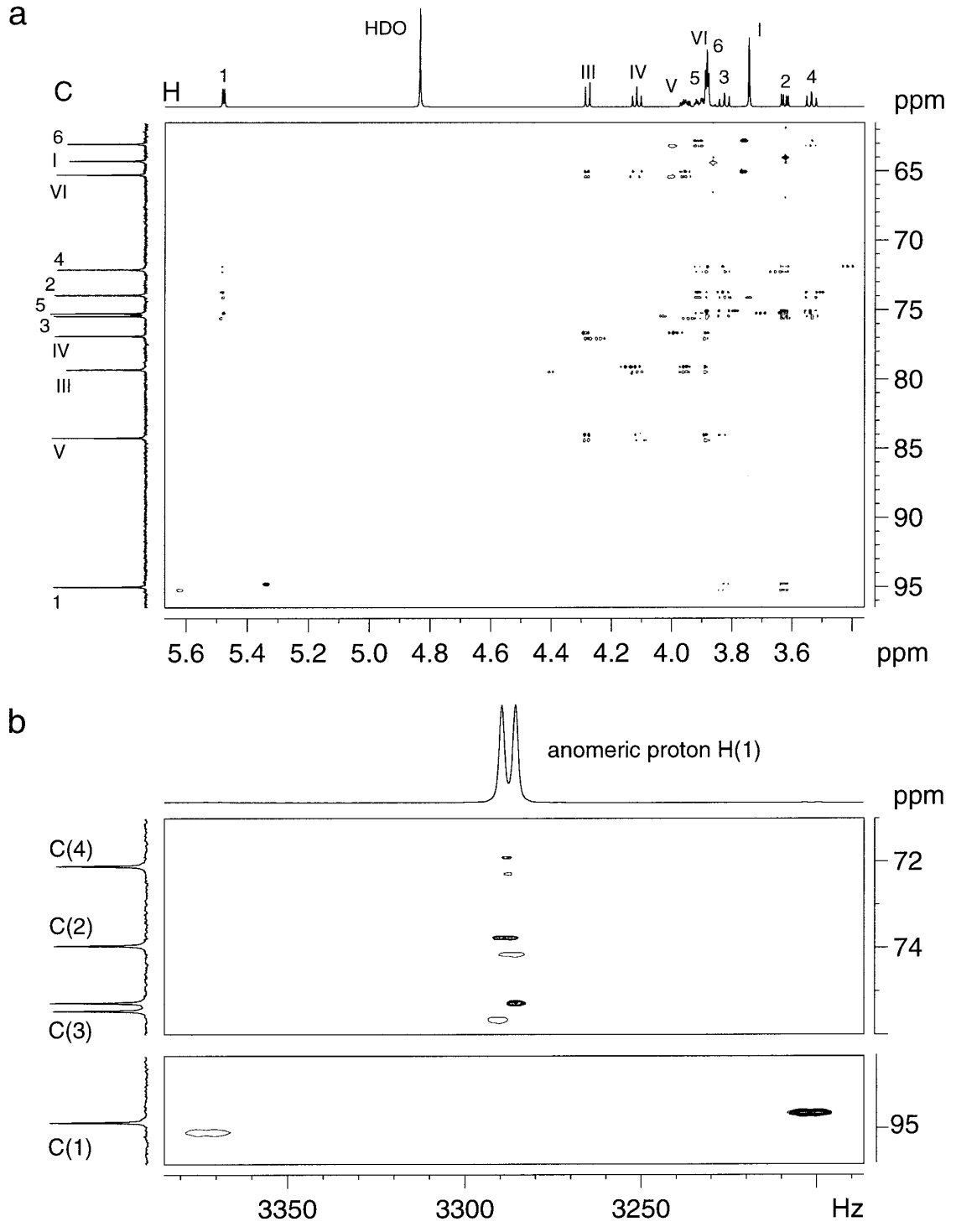

FIG. 4. (a) HECADE spectrum obtained from a sucrose solution in D_2O with the sequence of Fig. 3a. (b) Expansion of the cross peaks of the anomeric proton. Projections over each cross peak yield the active heteronuclear coupling in antiphase in both dimensions. In contrast, the homonuclear proton couplings are exclusively displayed in the proton dimension (F_2). Since the one-bond coupling can be assumed to be positive (*47*, *48*), the signs of the other couplings result from the tilt of the respective cross-peak pattern. For negative peaks, only one contour level was plotted.

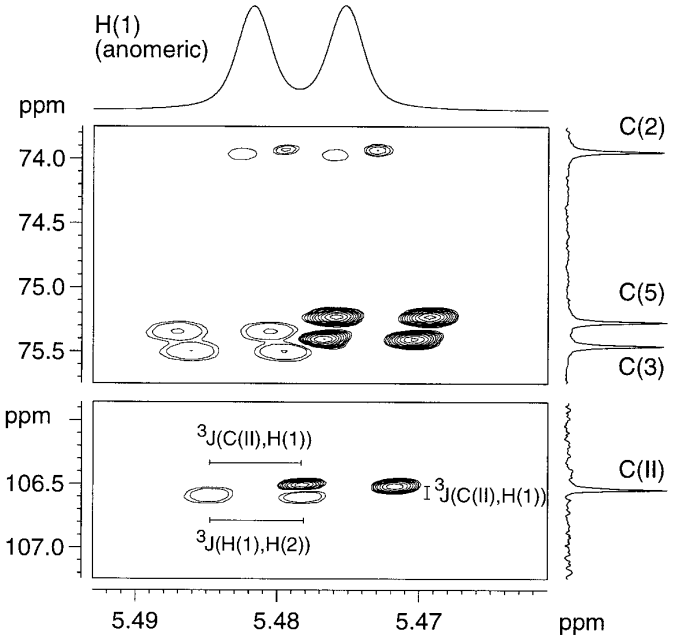

FIG. 5. Expansions from a sucrose spectrum measured with sequence (b) in Fig. 3. The optional isotropic mixing was not applied. For negative peaks, only a few intensity levels were plotted. Note the well-resolved correlation signals for C(3) and C(5). The following coupling-constant values were read from the spectrum: ^3J[C(II), H(1)] = +3.8 Hz, ^3J[C(3), H(1)] = +5.5 Hz, ^3J[C(5), H(1)] = +6.7 Hz, ^2J[C(2), H(1)] = +1.8 Hz. ^3J[H(1), H(2)] was found to be 3.9 Hz. Due to the respective scaling of interactions in the selective experiments 3b and 6b, accurate values for the coupling constants can be read from both the F_2 and the F_1 dimension.

$$\begin{aligned} A_1 &= I_x \cos(\omega_S t_1)\sin(\pi J_{IS} t_1^*), \\ B_1 &= 2I_y S_z \cos(\omega_S t_1)\cos(\pi J_{IS} t_1^*) \\ A_2 &= \mp I_y \sin(\omega_S t_1)\sin(\pi J_{IS} t_1^*), \\ B_2 &= \pm 2I_x S_z \sin(\omega_S t_1)\cos(\pi J_{IS} t_1^*). \end{aligned} \quad [2]$$

Apart from the phase in F_2 and the factor of 2 these terms are identical to those of Eq. [1]. In contrast to the above experiments, however, the A and B terms are acquired in separate scans. Depending on φ_4 the heteronuclear couplings either evolve during the first and last delay Δ or are refocused. Thus, either the A or the B terms are present at point c. By the phase-cycling procedures given in Table 2 the terms are combined in the proper way to generate pure-phase tilted cross-peak patterns, so that the sensitivity improvement for IS systems is preserved. This new approach to tilted cross-peak patterns depends on a uniform magnitude of the heteronuclear one-bond couplings. Artifacts due to nonuniform couplings can partly be purged by the cycling of φ_7 in the optional last composite S pulse (*40*).

When sequences (a) and (c) are compared, the latter implements a sensitivity-enhancement element but is sensitive to artifacts caused by nonuniform one-bond I, S coupling constants. For sequences (a) and (c) it will often be advantageous to choose the t_1^* increment in(t_1^*) smaller than the t_1 increment in(t_1). Thus the splittings caused by one-bond couplings are reduced relative to S-spin chemical-shift differences which facilitates interpretation. In contrast, for long-range experiments with sequence (b), the preferred choice is in(t_1^*) > in(t_1) to achieve a maximum coupling splitting in F_1. By a careful tuning of the increment ratio, signal overlap in F_1 can be reduced.

HSQC-BASED HECADE PULSE SEQUENCES

Since both pulse-sequence families that yield heteronuclear correlations with high sensitivity, HMQC/HMBC and HSQC experiments, exhibit intrinsic advantages, the HMQC-based sequences of Fig. 3 were adapted to perform S-spin single-quantum selection. The resulting sequences are displayed in Fig. 6. In analogy to Fig. 3, sequence 6a represents a single-bond correlation experiment with subsequent I-spin transfer, sequence 6b allows for heteronuclear long-range transfers, and sequence 6c is a sensitivity-enhanced version of sequence 6a. In order to obtain simple doublets at natural isotope abundance, I-spin coherences, not S-spin coherences, are again allowed to evolve under the heteronuclear coupling during t_1^*. The t_1^* evolution period is cut in two halves by a refocusing element R. In 6a and 6c, this is a BIRD$_x$ pulse, while for 6b selective π(I) pulses are used. In exact analogy to Fig. 3, the phase cycling for sequences 6a and 6b is given in Table 1, whereas for 6c it is listed in Table 2. Furthermore, the discussion of sequences 6a and 6b in terms of relevant density-operator components exactly follows that of 3a and 3b since the same terms are present at point b in the sequences. The same holds for point c in sequences 6c and 3c—provided that the phase acquired due to the pulsed field gradients is neglected. In sequence 6a, the HSQC correlation element is followed by a heteronuclear J-resolved experiment and a TOCSY transfer. Despite possi-

TABLE 2
Basic Phase Cycle for Experiments (c) in Figs. 3 and 6

Scan No.	φ_1	φ_4	φ_6	φ_7	φ_R
1e	0	2	3	2	0
1a	0	2	1	2	0
2e	0	2	3	3	0
2a	0	2	1	3	0
3e	1	3	3	2	1
3a	1	3	1	2	1
4e	1	3	3	3	3
4a	1	3	1	3	3

Note. For subsequent scans (e.g., 1e and 1a) the sign of gradients 1 and 2 is reversed. Note that if the TOCSY transfer and the additional π(I) pulse of the gradient echo are omitted, the echo and antiecho scans are exchanged which requires an inversion of the sign of φ_6 ($\varphi_2 = \varphi_5 = 0$.)

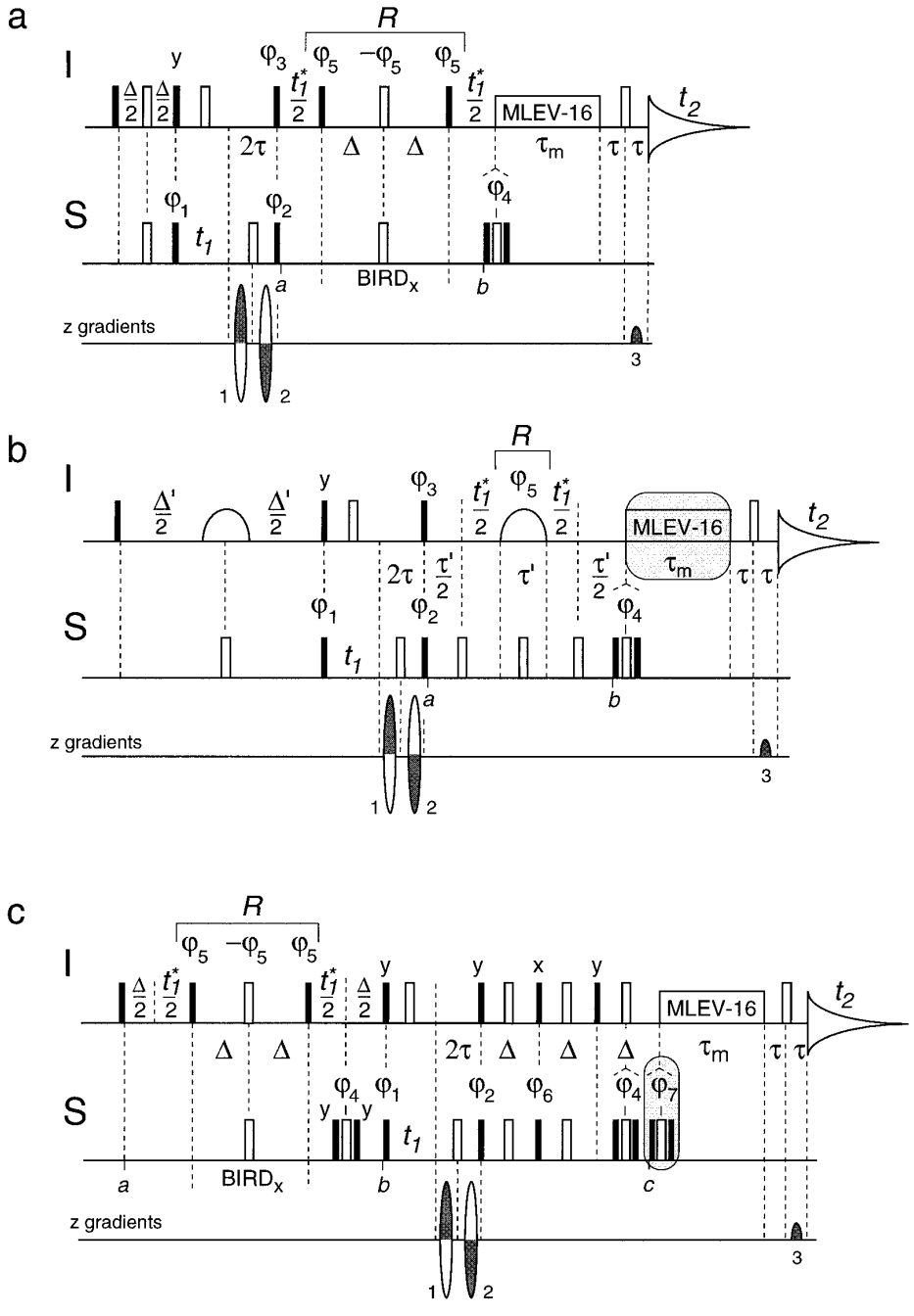

FIG. 6. HSQC-based pulse sequences for the determination of heteronuclear coupling constants from tilted E.COSY-type cross peaks, phase sensitive using the echo–antiecho method. For an explanation of the pulse-sequence symbols see the legend to Fig. 2. The value of τ' corresponds to the duration of the selective π(I) pulse. Phase cycles are listed in Tables 1 and 2. All sequences generate an ASSCI F_1 domain (cf. legend to Fig. 1 and text) that displays the active heteronuclear coupling splitting centered at the S-spin chemical-shift position.

ble diffusion processes during the long time between coherence defocusing and refocusing, the displayed position of the pulsed field gradients was found to be advantageous. Good artifact suppression and no significant loss of signal intensity were obtained with the sucrose sample. In 6b the first π(I) pulse is implemented as a selective pulse to achieve an INEPT transfer that is not disturbed by homonuclear I-spin couplings (*41*). In the heteronuclear *J*-resolved part of the experiment, the evolution of the heteronuclear coupling during the second selective π(I) pulse is refocused during the additional $\tau_1'/2$ periods. Thus a ''clean'' first experiment with $t_1^* = 0$ can be measured. In the sensitivity-enhanced version 6c, the heteronuclear *J*-resolved part of the sequence is shifted in front of the HSQC part. Here, the favorable tilt of the multiplets is constructed in exactly the same way as in sequence 3c.

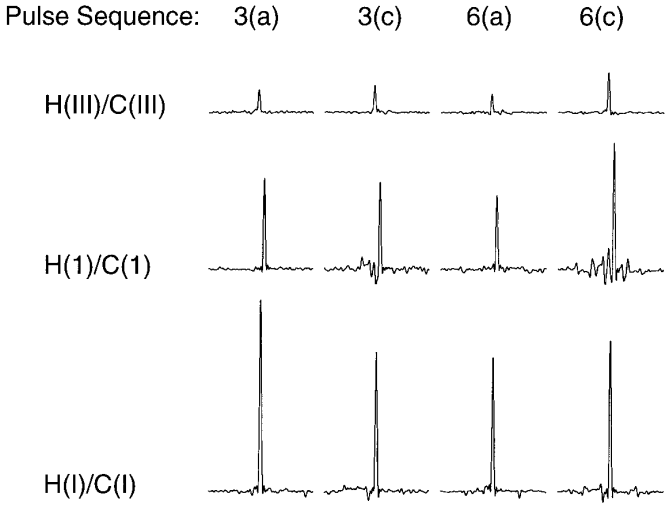

FIG. 7. Comparison of signal intensities in F_1 traces of sucrose HECADE spectra obtained with four sequences displayed in Figs. 3 and 6. The signal-intensity variation caused by different pulse sequences can only be compared for a given cross peak; i.e., these variations are found in rows of the picture. In a given column the intensity varies predominantly due to the rate of the polarization transfer under the isotropic mixing.

COMPARISON OF THE HECADE SEQUENCES

In Fig. 7 the signal intensities obtained with four different HECADE pulse sequences are compared for three selected cross peaks of two IS pairs and one I_2S group. For the H(III)/(C(III) pair with a ^1J(C,H) coupling of 144.2 Hz, the delays Δ were nearly perfectly optimized, whereas the anomeric proton H(1) displays a somewhat larger coupling of 169.5 Hz. Theoretically, due to the optimization of the sensitivity enhancement for the IS groups, no increase of the H(I)/C(I) peak intensity (I_2S group) is expected.

For the basic HMQC- and HSQC-based sequences, 3a and 6a, respectively, the HMQC version was found to consistently display somewhat better signal intensity. In contrast, in the sensitivity-enhanced versions 3c and 6c, the HSQC-based experiment performed better. Here, a consistent enhancement of the IS signals was found, whereas in the HMQC-based versions, the signal intensity in the enhanced versions was either only slightly increased [H(III)/C(III)] or even decreased [H(1)/C(1) and H(1)/C(1)]. The slight increase of the H(I)/C(I) cross peak in experiment 6c compared to 6a is not explained and possibly indicates the limited accuracy and reproducibility of such comparisons. In the sensitivity-enhanced sequences, larger artifacts in F_1 traces taken through the cross peaks of the strongly coupled CH_2 groups and of the anomeric CH group were found, as seen in Fig. 7. Since, in the HMQC-based experiments, all time periods between points *a* and *b* must occur symmetrically prior and after the refocusing element *R*, these sequences tend to be longer. For example, the maximum time between initial excitation and detection for our experiments 3a and 6a was 153 and 247 ms, respectively. Assuming a hypothetical constant relaxation with a time constant of 250 ms during this period, the signal intensity in the last FID should be larger by a factor of about 1.5 in the HSQC experiment. However, as is also clear from the experiments, many other factors are important.

CONCLUSIONS

The pulse-sequence family HECADE was found to rapidly yield a large number of heteronuclear short- and long-range coupling constants with relatively high sensitivity. The tilted display of the active coupling allows an accurate determination of heteronuclear coupling splittings from F_2 traces even when the linewidth of the resonances is of comparable magnitude to the coupling. The simplest HMQC-based HECADE experiments, 3a and 3b, seem most appropriate for routine use with small molecules. Sequence 3b should primarily be chosen when the active coupling of interest, e.g., of a proton with a quaternary carbon, is small in comparison with homonuclear I-spin couplings. With 3b, in contrast to 3a, long-range heteronuclear couplings are obtained even without the homonuclear TOCSY transfer. The potential of sequence 3b is greatly enhanced when, instead of multiplet-selective π(I) pulses, spectral-region-selective pulses can be employed. Provided that the affected I spins do not exhibit mutual couplings, 2D correlations of quite large spectral regions will still display pure phases (*26*). The HSQC-based pulse sequences are shorter, which may possibly be an advantage when working with faster relaxing samples. In addition, sensitivity enhancement was found to work well with HSQC-based sequences, whereas no significant enhancement was found for the HMQC-based variants. In both cases, the different approach to tilted active-coupling patterns in the sensitivity-enhanced sequences was found to produce more artifacts, which makes these sequences less attractive—unless the sensitivity gain is crucial. The ASSCI pulse-sequence element presents unique possibilities to flexibly control the appearance of the spectra. The implementation of the HECSII pulse-sequence element allows routine measurements of HMQC/HMBC spectra with pure phase and improved resolution. Both ASSCI and HECSII elements as well as active-coupling-pattern tilting are expected to be useful tools in a wide variety of pulse sequences.

EXPERIMENTAL

All spectra were measured in about seven hours with a 0.06 *M* D_2O solution of sucrose at 300 K on a Bruker AMX-600 spectrometer equipped with a 10 A gradient unit BGU-1 and a standard inverse triple-resonance $^1H/^{13}C/^{15}N$ probe with an actively shielded *z*-gradient coil. Proton and carbon $\pi/2$ pulse lengths were 10 and 15.5 μs, respectively. Eight FIDs were coherently added for each echo and antiecho data set for 512 t_1/t_1^* increments. The maximum t_1 value was 59.5 ms in all experiments; t_1^* was incremented up to 23.8 ms in experiments with one-bond heteronuclear polarization transfer to reduce the heteronuclear coupling splittings in F_1 by

a factor of 2.5 relative to carbon chemical-shift differences. In the selective experiments 3b and 6b, the maximum t_1^* value was 148.8 ms to increase the coupling separation in comparison with the shift differences; t_2 was sampled up to 1 s. The data matrices were weighted with a shifted sine window function in t_2 and zero-filled by a factor of 2 or 4 in both dimensions prior to 2D Fourier transformation. The delays Δ and Δ' were set to 3.57 and 71.4 ms, respectively, which corresponds to an optimization for a heteronuclear coupling of 140 and 7 Hz, neglecting relaxation. The interval τ, which includes the duration of a sine-shaped gradient pulse (1.5 ms) and a recovery time, was 1.7 ms. The gradient-amplitude ratio for the isotopomer-selection pulses 1, 2, and 3 was ± 2: ∓ 2:1. The two gradient pulses in the optional field-gradient pulse pairs flanking either the central selective π(I) pulse (sequence 3b) or the MLEV-16 sequence (*42*) (3a and 3b) each had a relative amplitude of 0.75. Isotropic mixing was applied for 56 ms with a field strength $B_{RF} = 2\pi \times 10$ kHz/γ_H. For the HECADE experiments, phases φ_2 and φ_5 were kept constant (x). For selective refocusing, a $\tau' = 15$ ms RE-BURP π(I) pulse was employed (*43*).

Note added in proof. While this article was in press further examples of ASSCI-domain experiments have been reported both with (*49*) and without (*50*) isolation of the coupling of interest in the ASSCI domain.

ACKNOWLEDGMENTS

This work was supported by the Swiss National Science Foundation and the Dr. Helmut Legerlotz-Stiftung. We thank O. Zerbe for valuable comments on the manuscript and W. von Philipsborn for his continuous interest and support.

REFERENCES

1. M. Eberstadt, G., Gemmecker, D. F. Mierke, and H. Kessler, *Angew. Chem. Int. Ed. Engl.* **34,** 1671 (1995).
2. C. Griesinger, O. W. Sørensen, and R. R. Ernst, *J. Chem. Phys.* **85,** 6837 (1986).
3. L. Müller, *J. Am. Chem. Soc.* **101,** 4481 (1979).
4. M. R. Bendall, D. T. Pegg, and D. M. Doddrell, *J. Magn. Reson.* **52,** 81 (1983).
5. A. Bax, R. H. Griffey, and B. L. Hawkins, *J. Magn. Reson.* **55,** 301 (1983).
6. A. Bax and M. F. Summers, *J. Am. Chem. Soc.* **108,** 2093 (1986).
7. G. Bodenhausen and D. J. Ruben, *Chem. Phys. Lett.* **69,** 185 (1980).
8. M. Kurz, P. Schmieder, and H. Kessler, *Angew. Chem. Int. Ed. Engl.* **30,** 1329 (1991).
9. U. Wollborn and D. Leibfritz, *J. Magn. Reson.* **98,** 142 (1992).
10. J. R. Garbow, D. P. Weitekamp, and A. Pines, *Chem. Phys. Lett.* **93,** 504 (1982).
11. A. Bax, *J. Magn. Reson.* **53,** 517 (1983).
12. A. Bax and S. Subramanian, *J. Magn. Reson.* **67,** 565 (1986).
13. M. Sattler, H. Schwalbe, and C. Griesinger, *J. Am. Chem. Soc.* **114,** 1126 (1992).
14. J. Lee, J. Fejzo, and G. Wagner, *J. Magn. Reson. B.* **102,** 322 (1993).
15. G. Otting, B. A. Messerle, and L. P. Soler, *J. Am. Chem. Soc.* **118,** 5096 (1996).
16. G. Bodenhausen and R. R. Ernst, *J. Magn. Reson.* **45,** 367 (1981).
17. G. Bodenhausen and R. R. Ernst, *J. Am. Chem. Soc.* **104,** 1304 (1982).
18. L. E. Kay and J. H. Prestegard, *J. Magn. Reson.* **77,** 599 (1988).
19. A. M. Mandel and A. G. Palmer III, *J. Magn. Reson. A* **110,** 62 (1994).
20. T. Szyperski, G. Wider, J. H. Bushweller, and K. Wüthrich, *J. Am. Chem. Soc.* **115,** 9307 (1993).
21. T. Szyperski, D. Braun, C. Fernández, C. Bartels, and K. Wüthrich, *J. Magn. Reson. B* **108,** 197 (1995).
22. T. Szyperski, D., Braun, C. Fernández, C. Bartels, and K. Wüthrich, *J. Magn. Reson. B* **109,** 339 (1995).
23. B. Brutscher, J.-P. Simorre, M. S. Caffrey, and D. Marion, *J. Magn. Reson. B* **105,** 77 (1994).
24. W. Koźmiński, D. Sperandio, and D. Nanz, *Magn. Reson. Chem.* **34,** 311 (1996).
25. W. Koźmiński and D. Nanz, *J. Magn. Reson. A* **122,** 245 (1996).
26. V. V. Krishnamurthy, *J. Magn. Reson. A* **121,** 33 (1996).
27. A. Bax, K. A. Farley, and G. S. Walker, *J. Magn. Reson. A* **119,** 134 (1996).
28. H. Kessler, M. Gehrke, and C. Griesinger, *Angew. Chem. Int. Ed. Engl.* **27,** 490 (1988).
29. C. Emetarom, T.-L. Hwang, G. Mackin, and A. J. Shaka, *J. Magn. Reson. A* **115,** 137 (1995).
30. L. Braunschweiler and R. R. Ernst, *J. Magn. Reson.* **53,** 521 (1983).
31. A. Bax, D. G. Davies, and S. K. Sarkar, *J. Magn. Reson.* **63,** 230 (1985).
32. M. H. Levitt and R. Freeman, *J. Magn. Reson.* **33,** 473 (1980).
33. O. Zerbe, J. H. Welsh, J. A. Robinson, and W. v. Philipsborn, *J. Magn. Reson.* **100,** 329 (1992).
34. E. Wörgötter, G. Wagner, and K. Wüthrich, *J. Am. Chem. Soc.* **108,** 6162 (1986).
35. P. Bachmann, W. P. Aue, L. Müller, and R. R. Ernst, *J. Magn. Reson.* **28,** 29 (1977).
36. J. Cavanagh, A. G. Palmer III, P. E. Wright, and M. Rance, *J. Magn. Reson.* **91,** 429 (1991).
37. L. E. Kay, P. Keifer, and T. Saarinen, *J. Am. Chem. Soc.* **114,** 10663 (1992).
38. G. Kontaxis, J. Stonehouse, E. D. Laue, and J. Keeler, *J. Magn. Reson. A* **111,** 70 (1994).
39. J. Schleucher, M. Schwendinger, M. Sattler, P. Schmidt, O. Schedletzky, S. J. Glaser, O. W. Sørensen, and C. Griesinger, *J. Biomol. NMR* **4,** 301 (1994).
40. O. W. Sørensen and R. R. Ernst, *J. Magn. Reson.* **51,** 477 (1983).
41. A. Bax, *J. Magn. Reson.* **57,** 314 (1984).
42. M. H. Levitt, R. Freeman, and T. Frenkiel, *J. Magn. Reson.* **47,** 328 (1982).
43. H. Geen and R. Freeman, *J. Magn. Reson.* **93,** 93 (1991).
44. J. Boyd, N. Soffe, B. John, D. Plant, and R. Hurd, *J. Magn. Reson.* **98,** 660 (1992).
45. J. R. Tolman, J. Chung, and J. H. Prestegard, *J. Magn. Reson.* **98,** 462 (1992).
46. R. E. Hurd, *J. Magn. Reson.* **87,** 422 (1990).
47. E. F. Mooney and P. H. Winson, *Annu. Rev. NMR Spectrosc.* **2,** 153 (1969).
48. J. H. Goldstein, V. S. Watts, and L. S. Rattet, *Prog. NMR Spectrosc.* **8,** 103 (1972).
49. V. V. Krishnamurthy, *J. Magn. Reson. B* **113,** 46 (1996).
50. J. R. Tolman and J. H. Prestegard, *J. Magn. Reson. B* **112,** 269 (1996).